

Supporting Information

Critical Properties of Aluminum

Divesh Bhatt, Ahren W. Jasper, Nate E. Schultz, J. Ilja Siepmann,*
and Donald G. Truhlar*

*Department of Chemistry and Minnesota Supercomputing Institute,
University of Minnesota, 207 Pleasant Street SE, Minneapolis, MN 55455-0431*

This document provides supporting information for an article to be published in the *Journal of the American Chemical Society*. It was prepared on January 30, 2006.

Table of Contents

1. Potential Models	2
2. Use of Born-Oppenheimer Approximation for Metals	4
3. Simulation and Analysis Methods	5
4. Numerical Results and Deviations from the Ideal-Gas Law	6
References	7
Tables	9
Figure	13

*To whom correspondence should be addressed. Email: siepmann@umn.edu, truhlar@umn.edu

1. Potential Models

In the last twenty years, analytic embedded-atom potentials¹ have gained wide use in simulations of metals. In the embedded-atom approximation, the total energy of a system of N interacting atoms is given by

$$U = \sum_{i>j}^N \phi(r_{ij}) + \sum_i^N F(\rho_i) \quad (\text{S1})$$

where r_{ij} is the distance between two atoms, ϕ is a pairwise additive repulsive term, F is an attractive many-body embedded-atom part, and ρ_i is a nonlinear function of the distances of atom i from the other atoms. The specific forms of ϕ , ρ_i , and F for the embedded-atom potentials parametrized to bulk solid-state data by Mei and Davenport² (called MDEA) and to nanoparticle and bulk energies by Jasper *et al.*³ (called NP-B) can be found in the original references.^{2,3}

The MDEA potential was originally parameterized to reproduce solid-state properties, whereas the NP-B potential was parameterized using geometries and energies for clusters and nanoparticles, as well as bulk properties. Here we review those parameterizations and discuss their applicability to the simulations presented in the paper. We have also included the NP-A⁴ potential in this summary, because the NP-A potential was fit using the same strategy as was used to obtain the NP-B potential, and it is generally more accurate than the NP-B potential for the test set, but more expensive to evaluate.

For solid-state simulations, an important test of an analytic potential energy function is how well it can predict the cohesive energy (E_{coh}), lattice constant (a_e), and bulk modulus (B_e). (In addition to the bulk modulus, one may also consider the individual components of the stress tensor, but we do not do so here.) Some care must be taken when comparing equilibrium properties predicted by an analytic potential energy surface with experimentally determined properties, which include thermal averaging and zero-point effects. Recently, Gaudion *et al.*⁵ analyzed experimental data for bulk aluminum and removed thermal and zero-point effects to obtain estimates for the bulk properties corresponding to the classical equilibrium structure. These adjusted values are shown in Table S1 and may be directly

compared with properties predicted by the analytic potential energy surfaces (or by electronic structure calculations, if the Born-Oppenheimer approximation is assumed valid—see Section 2 of this supporting information). There are no experimentally determined properties for the HCP and BCC crystal structures of aluminum, and for these values we scaled the DFT results of Jaffe *et al.*⁶ In particular, their computed HCP and BCC cohesive energies were then scaled by the ratio of experimental and calculated FCC cohesive energies.

Predictions of the bulk properties for the three analytic potential energy functions are compared to the accurate values in Table S1. All the potentials do well for lattice constants and cohesive energies. The NP-B potential was not fit to the FCC bulk modulus and overestimates it by 106%, whereas the MDEA potential was fit to the bulk modulus and has an error of 6%. The MDEA potential is qualitatively incorrect in its prediction of the relative stability of the different crystal structures for aluminum, predicting nearly equal cohesive energies for the FCC and HCP structures. These structural trends have been recognized in the literature as difficult to reproduce using the kind of simple analytic potential energy functions considered here. The NP-B potential, however, predicts the FCC-HCP gap with the correct order of magnitude, although it is underestimated.

The fitting strategy used to obtain the NP-A and NP-B potentials was designed to produce potentials that are accurate for systems smaller than the bulk, in particular for systems sizes all the way down to Al_2 . In a previous paper,⁴ we presented a database of energies for Al clusters and nanoparticles. The largest cluster that we considered was Al_{177} , which is a 2 nm particle. In Table S2, we present mean unsigned errors for the NP-A, NP-B, and MDEA potentials for the various particle size ranges. The most accurate potential is the NP-A potential, which is accurate for clusters, nanoparticles, and bulk properties. The NP-B potential is only slightly less accurate than the NP-A potential, whereas the MDEA potential, which was not intended to be used for cluster or nanoparticle simulations and was not fit to cluster or nanoparticle data, is about 7 times less accurate than the NP-B potential for dimers and trimers and about 2 times less accurate for nanoparticles with 89 to 177 particles.

As discussed in the paper, simulations using the NP-B and MDEA potentials were shown to be sensitive to the quality of the potential in the small-cluster limit. The NP-B potential does not predict significant gas-phase clustering of Al atoms for temperatures less than 2000 K, whereas the MDEA potential predicts a high degree of clustering in the gas phase for these temperatures. This clustering is attributed to an overestimation of the bond strengths for small clusters for MDEA. For example, the bond strength for Al_2 , when calculated with accurate DFT, NP-A, NP-B, and MDEA is 1.56, 1.55, 1.94, and 4.25 eV, respectively, as compared to the accurate value of 1.44 eV.⁷

2. Use of Born-Oppenheimer Approximation for Metals

The question sometimes arises of whether one can use the Born-Oppenheimer approximation for processes involving metals, and clearly this requires justification.^{8,9} As pointed out in a recent review, most theoretical treatments of gas-phase and condensed-phase dynamics, including metals, are based on the Born-Oppenheimer approximation, but this cannot be justified for metals on the picosecond time scale.¹⁰ Similarly most computational thermochemistry, even for metals, is based on the Born-Oppenheimer approximation, which means that only a single potential energy surface, and hence a unique potential energy function, is considered. This widely used model is also employed here, and thus the potential energy function, which is fit in part to bulk metal properties like the cohesive energy, is in some sense an “effective” potential. Although such potential functions are justified in part by their empirical success (otherwise they would not be used so widely), it would be desirable in future work to include the effect of low-energy electronic states directly and to study how well and how transferably these effects can be represented by an effective potential. We note, with regard to such future work, that the effect of excited electronic states will be quantitatively different for bulk metals, for nanoparticles, for clusters, and for critical properties.

3. Simulation and Analysis Methods

The vapor-liquid coexistence curve is determined for the MDEA and NP-B potentials using Gibbs ensemble Monte Carlo (GEMC).^{11,12} GEMC utilizes two separate simulation boxes that are in thermodynamic contact, but do not have an explicit interface. In addition to conventional Monte Carlo moves, particle and volume exchanges between the two boxes allow one to establish thermal, phase, and mechanical equilibrium, respectively. As a result, for a given state point the properties of the coexisting phases can be determined directly from a single simulation. A total of 350 atoms is used for most of the GEMC simulations with the overall system volume adjusted so that about 50-100 particles are found in the vapor phase. After equilibration periods consisting of at least 1.5×10^7 MC moves, averages are collected over at least 3.5×10^7 moves. An additional canonical ensemble simulation is carried out at the vapor density obtained from GEMC, and the equilibrium vapor pressure at each temperature is obtained by using the thermodynamic definition of pressure.¹³ To determine the effect of the system size, additional GEMC simulations were performed for 800 atoms at the two highest temperatures for the NP-B potential (5000 and 5250 K). For the larger system size, the equilibration period is 1.6×10^7 MC moves, and averages are collected over 4×10^8 MC moves.

Two extrapolation methods are used to estimate the critical temperatures and densities from the GEMC results. In the first method, the critical temperature, T_c , is estimated using a weighted fit of the simulation data above the boiling point to the density scaling law¹² with an Ising critical exponent of 0.325. Once the critical temperature is known, the critical density is obtained from the law of rectilinear diameters.¹² The other approach is similar, but it uses additional terms in the scaling and rectilinear laws to account for deviations from the corresponding states.¹⁴ The critical constants for either potential presented in this work are the averages of the estimates obtained from these two methods. The critical pressure is computed from a separate canonical-ensemble simulation at T_c and ρ_c . The normal boiling point is obtained from a Clausius-Clapeyron¹⁵ fit to the saturated vapor pressure of the four GEMC simulations that yield a pressure close to 1 atm.

4. Numerical Results and Deviations from the Ideal-Gas Law

Tables S3 and S4 summarize the GEMC data calculated for the systems with 350 atoms using the NP-B and MDEA potentials, respectively. Standard deviations for the saturated liquid and vapor densities, the saturated vapor pressures, and heats of vaporization are obtained by dividing the total number of samples into 10 blocks. At the two highest temperatures, GEMC simulations for the NP-B potential were carried out for two system sizes. The coexistence densities for the 350- and 800-atom systems agree to within the statistical uncertainties. Thus, it appears that finite-size errors for the critical properties are smaller than those introduced by the procedures used to fit the coexistence curve. A rigorous finite-size scaling analysis¹⁶ is not possible for simulations in the Gibbs ensemble, but a comparison of simulation data for Lennard-Jonesium^{17,18,19} points to finite-size errors of less than 1% for the system size used here.

Figure S1 quantifies the deviation of the vapor-phase equation of state from the ideal-gas law over the entire range of simulated temperatures by plotting the compressibility factor, Z , given by

$$Z = \frac{p_v v}{RT} \quad (\text{S2})$$

where p_v is the vapor pressure, v is the molar volume, R is the ideal-gas constant, and T is the temperature. The NP-B vapor deviates significantly from an ideal gas only at higher temperatures. In contrast, the MDEA vapor phase is very nonideal even at temperatures close to the experimental triple point.

References

1. Daw, M. S.; Baskes, M. I. *Phys. Rev. Lett.* **1983**, *85*, 1285.
2. Mei, J.; Davenport, J. W. *Phys. Rev. B* **1992**, *46*, 21.
3. Jasper, A. W.; Staszewski, P.; Staszewska, G.; Schultz, N. E.; Truhlar, D. G. *J. Phys. Chem. B* **2004**, *108*, 8996.
4. Jasper, A. W.; Schultz, N. E.; Truhlar, D. G. *J. Phys. Chem. B* **2005**, *109*, 3915.
5. Gaudoin, R.; Foulkes, W. M. C. *Phys. Rev. B* **2002**, *66*, 052104.
6. Jaffe, J. E.; Kurtz, R. J.; Gutowski, M. *Comput. Mater. Sci.* **2000**, *18*, 199.
7. Zhan, C. G.; Zheng, F.; Dixon, D. A. *J. Am. Chem. Soc.* **2002**, *124*, 14795.
8. Chester, V. *Adv. Phys.* **1961**, *10*, 357.
9. Wonchoba, S. E.; Hu, W.-P.; Truhlar, D. G. In *Theoretical and Computational Approaches to Interfacial Phenomena*; Sellers H. L. and Golab, J. T. Eds. (Plenum: New York, 1994); pp. 1-34.
10. Tully, J. C. *Annu. Rev. Phys. Chem.* **2000**, *51*, 153.
11. Panagiotopoulos, A. Z. *Mol. Phys.* **1987**, *61*, 813.
12. Frenkel, D.; Smit, B. *Understanding Molecular Simulations* (Academic Press, San Diego, 1996); chapter 8.
13. Hummer, G.; Jensen, N. G.; Neumann, M. *J. Chem. Phys.* **1998**, *109*, 2791.
14. Sengers, J. V.; Level-Sengers, J. M. H. In *Progress in Liquid Physics*; Croxton, C. A., Ed. (Wiley: Chichester, 1978); pp. 103-174.
15. Clausius, R. *Poggendorff's Annalen der Physik und Chemie* **1850**, *79*, 368-397.

16. Wilding, N. B. *Phys. Rev. B* **1995**, 52, 602.
17. Potoff, J. J.; Panagiotopoulos, A. Z. *J. Chem. Phys.* **1998**, 109, 10914.
18. Smit, B. *J. Chem. Phys.* **1992**, 96, 8639.
19. Martin, M. G.; Siepmann, J. I. *J. Phys. Chem. B* **1998**, 102, 2569.

Tables

Table S1: The experimental and calculated cohesive energies (E_{coh}), lattice constants (a_e), and bulk modulus (B_e) given in eV/atom, Å, and eV/Å³, respectively.

Method	FCC			HCP	BCC
	E_{coh}	a_e	B_e^a	E_{coh}	E_{coh}
Accurate ^b	3.43	4.0217	0.507	3.39	3.33
NP-A	3.4278	4.0101	0.721	3.4158	3.3368
NP-B	3.4276	4.0334	1.054	3.4090	3.3505
MDEA	3.3900	4.0500	0.481	3.3859	3.3603

^aThe conversion factor from 10¹¹ N/m² to eV/Å³ is 0.62415.

^bAdjusted experimental values from Ref 5 for FCC, and scaled DFT results from Ref 6 for HCP and BCC.

Table S2: Mean unsigned errors (eV/atom) averaged over the data set presented in Ref 4.

Particle Size	NP-A	NP-B	MDEA
2	0.01	0.09	0.55
3	0.10	0.08	0.63
4	0.09	0.11	0.54
5-7	0.08	0.08	0.36
8-13	0.04	0.05	0.23
14-19	0.06	0.08	0.27
20-43	0.04	0.07	0.18
50-55	0.03	0.02	0.13
56-79	0.02	0.03	0.11
80-87	0.02	0.03	0.08
89-177	0.02	0.04	0.08
bulk	0.02	0.03	0.03
overall	0.03	0.05	0.16

Table S3: GEMC data obtained for the NP-B potential.

N	T (K)	ρ_l (kg/m ³)	ρ_v (kg/m ³)	p_v (kPa)	ΔH_{vap} (kJ/mol)
350	1100	2410 \pm 1	$(1.747 \pm 0.062) \times 10^{-10}$	$(5.92 \pm 0.21) \times 10^{-8}$	311
350	1200	2387 \pm 1	$(2.635 \pm 0.039) \times 10^{-9}$	$(9.71 \pm 0.15) \times 10^{-7}$	310
350	1350	2350 \pm 1	$(7.07 \pm 0.11) \times 10^{-8}$	$2.94 \pm 0.05 \times 10^{-5}$	309
350	1500	2320 \pm 1	$(1.035 \pm 0.021) \times 10^{-6}$	$(4.77 \pm 0.10) \times 10^{-4}$	307
350	2000	2210 \pm 1	$(3.497 \pm 0.051) \times 10^{-4}$	$(2.13 \pm 0.03) \times 10^{-1}$	300
350	2500	2110 \pm 1	$(1.078 \pm 0.013) \times 10^{-2}$	7.96 \pm 0.01	291
350	3000	2006 \pm 1	$(1.186 \pm 0.012) \times 10^{-1}$	$(9.89 \pm 0.13) \times 10$	276
350	4000	1790 \pm 1	2.883 \pm 0.043	$(2.52 \pm 0.07) \times 10^3$	229
350	4500	1670 \pm 1	9.25 \pm 0.23	$(7.52 \pm 0.34) \times 10^3$	200
350	5000	1536 \pm 1	$(3.55 \pm 0.17) \times 10^1$	$(2.02 \pm 0.27) \times 10^4$	145
350	5250	1462 \pm 2	$(1.12 \pm 0.11) \times 10^2$	$(3.2 \pm 1.9) \times 10^4$	89
800	5000	1537 \pm 1	$(3.69 \pm 0.11) \times 10^1$		
800	5250	1465 \pm 3	$(9.1 \pm 1.6) \times 10^1$		

Table S4: GEMC data obtained for the MDEA potential.

T (K)	ρ_l (kg/m ³)	ρ_v (kg/m ³)	p_v (kPa)	ΔH_{vap} (kJ/mol)
1100	2260 \pm 1	$(7.503 \pm 0.059) \times 10^{-8}$	$(1.23 \pm 0.04) \times 10^{-5}$	102
1200	2225 \pm 1	$(1.481 \pm 0.039) \times 10^{-6}$	$(2.56 \pm 0.05) \times 10^{-4}$	100
1500	2101 \pm 1	$(4.351 \pm 0.011) \times 10^{-3}$	$(8.64 \pm 0.16) \times 10^{-1}$	94
1600	2065 \pm 1	$(1.033 \pm 0.003) \times 10^{-1}$	$(2.30 \pm 0.04) \times 10^1$	87
1800	1984 \pm 1	$(3.549 \pm 0.036) \times 10^{-1}$	$(8.51 \pm 0.27) \times 10^1$	87
1900	1942 \pm 1	$(7.95 \pm 0.16) \times 10^{-1}$	$(1.96 \pm 0.11) \times 10^2$	85
2000	1899 \pm 1	$(1.442 \pm 0.027) \times 10^0$	$(3.65 \pm 0.21) \times 10^2$	82
2200	1809 \pm 1	$(4.15 \pm 0.10) \times 10^1$	$(1.07 \pm 0.08) \times 10^3$	77
2400	1714 \pm 1	$(1.063 \pm 0.043) \times 10^2$	$(2.61 \pm 0.35) \times 10^3$	69
2500	1664 \pm 2	$(1.754 \pm 0.092) \times 10^2$	$(4.20 \pm 0.77) \times 10^3$	65
2600	1606 \pm 2	$(3.05 \pm 0.20) \times 10^2$	$(6.6 \pm 1.7) \times 10^3$	57
2700	1553 \pm 3	$(5.64 \pm 0.35) \times 10^2$	$(9.8 \pm 3.1) \times 10^3$	46

Figure

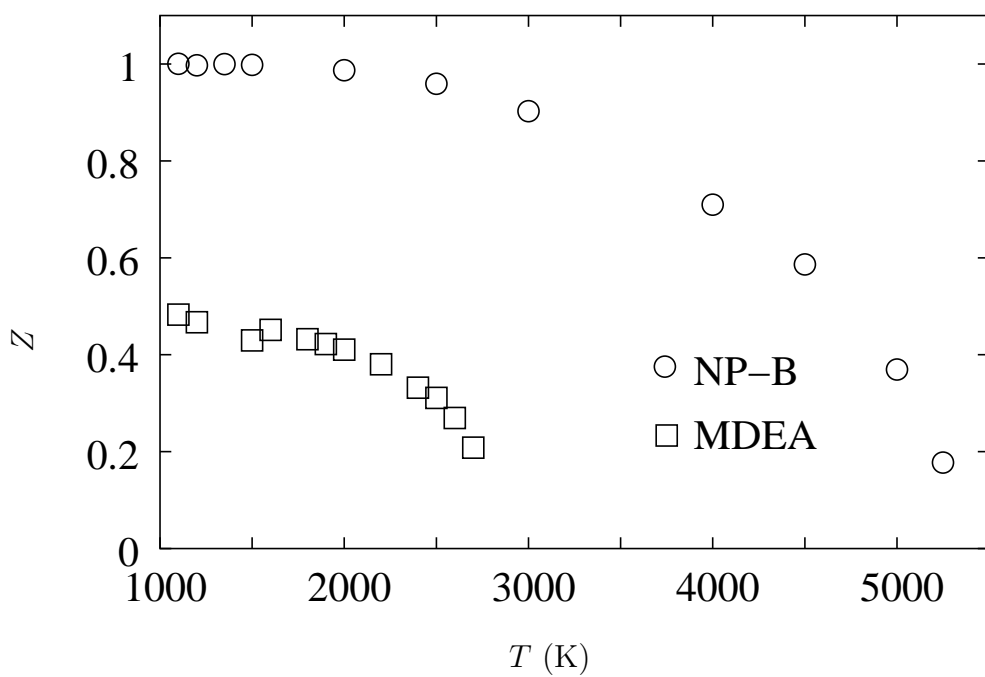


Figure S1: Temperature dependence of the compressibility factor for the saturated vapor phase calculated using the MDEA (squares) and NP-B (circles) potentials.